AFRL-OSR-VA-TR-2015-0030

Mathematical Problems in Imaging In Random Media

Beatrice Riviere
WILLIAM MARSH RICE UNIV HOUSTON TX

01/15/2015
Final Report

Air Force Research Laboratory
AF Office Of Scientific Research (AFOSR)/ RTB
Arlington, Virginia 22203
Air Force Materiel Command

REPORT DOCUMENTATION PAGE

Form Approved
OMB No. 0704-0188

1. REPORT DATE *(DD-MM-YYYY)*	**2. REPORT TYPE**	**3. DATES COVERED** *(From - To)*
13-01-2015	Final report	04/01/2012-03/31/2015

4. TITLE AND SUBTITLE

Mathematical Problems in Imaging in Random Media

5a. CONTRACT NUMBER

5b. GRANT NUMBER

FA9550-12-1-0117

5c. PROGRAM ELEMENT NUMBER

6. AUTHOR(S)

Liliana Borcea

5d. PROJECT NUMBER

5e. TASK NUMBER

5f. WORK UNIT NUMBER

7. PERFORMING ORGANIZATION NAME(S) AND ADDRESS(ES)

University of Michigan as a subcontractor to Rice University

8. PERFORMING ORGANIZATION REPORT NUMBER

9. SPONSORING / MONITORING AGENCY NAME(S) AND ADDRESS(ES)

DOD: Air Force Office of Scientific Research

10. SPONSOR/MONITOR'S ACRONYM(S)

11. SPONSOR/MONITOR'S REPORT NUMBER(S)

12. DISTRIBUTION / AVAILABILITY STATEMENT

Publicly available

13. SUPPLEMENTARY NOTES

14. ABSTRACT

We report our research results on the following topics:
- Sound and electromagnetic wave propagation in random waveguides
- Imaging in random waveguides.
- Wave propagation in time dependent random media.
- Synthetic Aperture Radar imaging with motion estimation.

15. SUBJECT TERMS

Wave propagation; imaging; wave scattering; random media

16. SECURITY CLASSIFICATION OF:			**17. LIMITATION OF ABSTRACT**	**18. NUMBER OF PAGES**	**19a. NAME OF RESPONSIBLE PERSON**
a. REPORT	**b. ABSTRACT**	**c. THIS PAGE**			Liliana Borcea
U	U	U	SAR	17	**19b. TELEPHONE NUMBER** *(include area code)* 7138846277

Final report for AFOSR grant FA9550-12-1-0117

Liliana Borcea

I. Research

We report in sections 1-4 the following published and submitted research results: (1) Quantification of net scattering effects in waveguides with random boundaries and filled with random media. (2) Imaging in random waveguides. (3) Pulse propagation in time dependent random media. (4) Synthetic Aperture Radar imaging with motion estimation. Then we mention in section 5 some current work.

1 Scattering effects in random waveguides

Random waveguides are mathematical models of waveguides with rough boundaries, filled with heterogeneous media. The microscale features (fluctuations of the boundaries and small inhomogeneities in the medium) cannot be known or determined in detail, they are necessarily uncertain. We study the propagation of this uncertainty to the wave field by placing the problem in a stochastic framework and analyzing the solution of the acoustic wave equation and Maxwell's equations in waveguides with random media and boundaries. The analysis is asymptotic in the limit $\varepsilon \to 0$, where ε is the scale of the amplitude of the random perturbations. It uses the diffusion limit theorem to obtain a mathematically rigorous characterization of the wave field at long ranges properly scaled by ε to see net cumulative scattering effects. The results describe in detail the randomization of the wave field, quantify the statistical decorrelation of its components and describe the transport of energy in the waveguide. They are the foundation of our new theory of robust imaging in random waveguides (section 2).

1.1 Two dimensional acoustic waveguides

We illustrate in Figure 1 the schematic of a two dimensional waveguide with boundaries

$$X_{_B}(z) = \varepsilon \mu_{_B}\left(\frac{z}{\ell}\right), \qquad X_{_T}(z) = X\left[1 + \varepsilon \mu_{_T}\left(\frac{z}{\ell}\right)\right], \tag{1}$$

where $\mu_{_B}$ and $\mu_{_T}$ are random processes with arguments scaled by the correlation length ℓ and X is the ideal waveguide depth. The waveguide is filled with a random medium with wave speed $c(\vec{\mathbf{x}})$ satisfying

$$\frac{1}{c^2(\vec{\mathbf{x}})} = \frac{1}{c_o^2}\left[1 + \varepsilon\, \nu\left(\frac{\vec{\mathbf{x}}}{\ell}\right)\right], \qquad \vec{\mathbf{x}} = (x, z), \tag{2}$$

with ν another mean zero random process. The results in [3, 4] characterize the statistics of the wave field $p(t, \vec{\mathbf{x}})$, the solution of the wave equation in the waveguide, with excitation given by a source with density $\rho(\vec{\mathbf{x}})$ compactly supported around range $z = 0$, emitting a pulse $f(t)$ with carrier frequency ω_o and bandwidth B. The analysis is under the assumption that the random processes ν, $\mu_{_B}$ and $\mu_{_T}$ are statistically independent, stationary in range and with z integrable autocorrelations $\mathcal{R}_\nu$, $\mathcal{R}_{_B}$ and $\mathcal{R}_{_T}$.

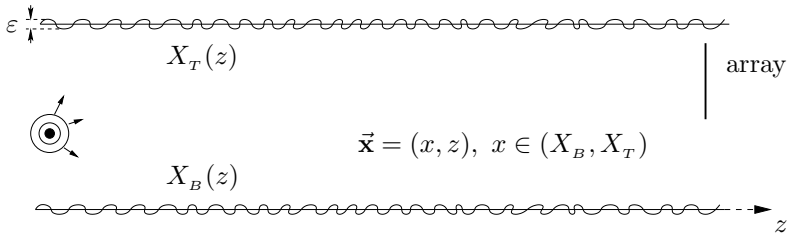

Figure 1: Schematic of a two dimensional waveguide. The waves emitted by a source are trapped by boundaries at cross-range $x = X_{_B}(z)$ and $x = X_{_T}(z)$ and propagate in the range direction z toward an array of sensors. The boundaries have small random fluctuations with amplitude scaled by ε and the waveguide is filled with a random medium.

To summarize the results, let us write the mode decomposition of the wave

$$p(t, \vec{\mathbf{x}}) = \int_{-\infty}^{\infty} \frac{d\omega}{2\pi B} \widehat{f}\left(\frac{\omega - \omega_o}{B}\right) e^{-i\omega t} \sum_{j=1}^{N(\omega)} \left[A_j(\omega, z)\phi_j(x)e^{i\beta_j(\omega)z} + B_j(\omega, z)\phi_j(x)e^{-i\beta_j(\omega)z}\right] + \text{evanescent} \tag{3}$$

where the hat denotes Fourier transform. The modes $\phi_j(x)e^{\pm i\beta_j(\omega)z - i\omega t}$ are special time harmonic solutions of the wave equation in ideal waveguides, and represent forward and backward going waves. They are defined by the eigenfunctions $\phi_j(x)$ of the operator $\partial_x^2 + k^2$, for whatever boundary conditions we have at $x = 0$ and X, where $k = \omega/c_o$. The mode wavenumbers β_j equal the square root of the eigenvalues, which are non-negative for $j = 1, \ldots, N(\omega)$, with integer $N(\omega) \approx \lfloor kX/\pi \rfloor$. The scattering effects are in the forward and backward mode amplitudes A_j and B_j, which are random fields. We can write them as

$$A_j(\omega, z) = \int d\vec{\mathbf{x}}'\, \rho(\vec{\mathbf{x}}')a_j(\omega, z, \vec{\mathbf{x}}')e^{-i\beta_j(\omega)z'}, \qquad B_j(\omega, z) = \int d\vec{\mathbf{x}}'\, \rho(\vec{\mathbf{x}}')b_j(\omega, z, \vec{\mathbf{x}}')e^{i\beta_j(\omega)z'}, \tag{4}$$

in terms of the amplitudes a_j and b_j of the modal expansion of the Green's function $G(t, \vec{\mathbf{x}}, \vec{\mathbf{x}}')$.

We explain in [3, 4] that if the waves do not travel too far, which means explicitly that $z \ll \varepsilon^{-2}\lambda_o$, where λ_o is the carrier wavelength, then

$$a_j(\omega, z, \vec{\mathbf{x}}') \approx a_{j,o}(\omega, x') := \frac{\phi_j(x')}{2i\beta_j(\omega)}, \qquad b_j(\omega, z, \vec{\mathbf{x}}') \approx 0, \quad 1 \le j \le N(\omega). \tag{5}$$

The random fluctuations in the waveguide are negligible at such ranges and the mode amplitudes (4) are deterministic and proportional to the Fourier coefficients of the source density

$$A_j(\omega, z) \approx \frac{1}{2i\beta_j(\omega)} \int_0^X dx\, \phi_j(x') \int_{-\infty}^{\infty} \rho(x', z')e^{-i\beta_j(\omega)z'} = \frac{\overline{\widehat{\rho}_j(\beta_j(\omega))}}{2i\beta_j(\omega)}, \qquad B_j(\omega, z) \approx 0. \tag{6}$$

The bar denotes complex conjugate and we use the term Fourier coefficients because $\phi_j(x)$ are normalized trigonometric functions.

The random fluctuations cause net scattering effects at ranges $z = \varepsilon^{-2}Z$, with $Z \gtrsim \lambda_o$. There we have

$$\begin{pmatrix} \mathbf{a}(\omega, z = \varepsilon^{-2}Z, \vec{\mathbf{x}}') \\ \mathbf{b}(\omega, z = \varepsilon^{-2}Z, \vec{\mathbf{x}}') \end{pmatrix} = \mathbb{P}^{\varepsilon}(\omega, Z, \vec{\mathbf{x}}') \begin{pmatrix} \mathbf{a}_o(\omega, x') \\ \mathbf{b}_o(\omega, x') \end{pmatrix}, \tag{7}$$

where $\mathbf{a}$ and $\mathbf{b}$ are the vectors with N components a_j and b_j, and $\mathbb{P}^{\varepsilon}$ is the $2N \times 2N$ propagator matrix. It models the mode mixing induced by scattering and is shown in [3, 4] that as $\varepsilon \to 0$ it converges[1] in

[1] This result is the extension to random boundaries of the analysis of Kohler and Papanicolaou [18] and of Dozier and Tappert [15], which is for waveguides filled with random media but flat boundaries.

distribution to a random Markov diffusion $\mathbb{P}$ whose generator can be computed explicitly in terms of the autocorrelations $\mathcal{R}_\nu$, $\mathcal{R}_{_B}$ and $\mathcal{R}_{_T}$ of the fluctuations in the waveguide. The significance of this result is that we can approximate explicitly all the statistical moments of the wavefield that we need. For imaging applications we study in particular the first and second moments. The first moment gives the coherent wave, the expectation of (3). The second moments describe the random fluctuations of (3) and the statistical decorrelation of its components over frequencies and modes. They also tell us how energy is transported by the modes in the waveguide.

It turns out that in regimes with $\ell \gtrsim \lambda_o$ and for smooth enough in z autocorrelations $\mathcal{R}_\nu$, $\mathcal{R}_{_B}$ and $\mathcal{R}_{_T}$, the backscattered waves are very weak and may be neglected. The evanescent waves interact with the forward going waves and have some small influence on the statistics of their amplitudes. This is rigorously taken into account in [3, 4] and the results summarized here. The coherent wave field is

$$\mathbb{E}\left[p(t,\vec{\mathbf{x}})\right] \approx \int_{-\infty}^{\infty} \frac{d\omega}{2\pi B}\widehat{f}\left(\frac{\omega-\omega_o}{B}\right)\sum_{j=1}^{N(\omega)}\mathbb{E}\left[A_j(\omega,z)\right]\phi_j(x)e^{i\beta_j(\omega)z-i\omega t}, \qquad z=\varepsilon^{-2}Z, \tag{8}$$

where $\mathbb{E}$ denotes expectation (mean) and

$$\mathbb{E}\left[A_j(\omega,z)\right] = \int d\vec{\mathbf{x}}'\rho(\vec{\mathbf{x}}')\mathbb{E}\left[a_j(\omega,z,\vec{\mathbf{x}}')\right]e^{-i\beta_j(\omega)z'} \approx \frac{\widehat{\rho}_j(\beta_j(\omega)}{2i\beta_j(\omega)}e^{-\frac{\varepsilon^2 z}{\mathcal{S}_j(\omega)}+i\frac{\varepsilon^{-2}z}{\mathcal{L}_j(\omega)}}. \tag{9}$$

The mean mode amplitudes differ from the amplitudes (6) in ideal waveguides by the decaying and oscillatory exponential. We have a dispersion effect manifested on the range scale $\varepsilon^{-2}\mathcal{L}_j(\omega)$ and an attenuation on the scale $\varepsilon^{-2}\mathcal{S}_j(\omega)$. Turns out that the energy of the modes $\mathbb{E}\left[|A_j|^2\right]$ remains finite no matter how large z is. Thus, the attenuation in (9) is a manifestation of the randomization (loss of coherence) of the modes, and $\mathcal{S}_j(\omega)$ is their scattering mean free path.

Both $\mathcal{S}_j$ and $\mathcal{L}_j$ are calculated explicitly in [3, 4]. For example, the scattering mean free paths are

$$\mathcal{S}_j = 2\left\{\sum_{q=1}^{N}\frac{k^4\ell}{4\beta_j\beta_q}\left[\frac{4(jq)^2}{N^4}\left(\widehat{\mathcal{R}}_{_B}+\widehat{\mathcal{R}}_{_T}\right)+\widehat{\mathcal{R}}_{\nu_{jq}}\right]\left(\ell\left(\beta_j-\beta_q\right)\right)\right\}^{-1}, \tag{10}$$

where $\mathcal{R}_{\nu_{jq}}$ is the autocorrelation of the stationary process

$$\nu_{jq}\left(\frac{z}{\ell}\right) = \int_0^X dx\,\nu\left(\frac{x}{\ell},\frac{z}{\ell}\right)\phi_j(x)\phi_q(x).$$

We display in Figure 1 the scales $\mathcal{S}_j(\omega_o)$ (blue line) and $\mathcal{L}_j(\omega_o)$ (green line) for two simplifications of equation (10): The first is for a waveguide with flat bottom and homogeneous medium where we keep only the $\widehat{\mathcal{R}}_{_T}$ term in (10). The second is for a waveguide with flat boundaries, where we keep only the $\widehat{\mathcal{R}}_{\nu_{jq}}$ term. We let $\mathcal{R}_{_T}$ be of Matérn 7-2 form, with $\ell = \lambda_o/\sqrt{5}$ and $\varepsilon = 1.3\%$. The autocorrelation $\mathcal{R}_\nu$ is Gaussian, with $\ell = \lambda_o$. The waveguide has $X = 20\lambda_o$ so $N(\omega_o) = 40$. The key point displayed in Figure 2, which turns out to be important for imaging, is that when scattering at the boundary dominates (left plot), there is a very strong mode dependence of the scales $\mathcal{S}_j$ and $\mathcal{L}_j$. In particular, the first modes which travel faster in range can go $10^5\lambda_o$ before they randomize, whereas the slow modes with index $j \approx N$ randomize on ranges of the order λ_o. If the random medium plays the important role (right plot), then the last modes still randomize on range scales of order λ_o, but there is a much weaker mode dependence of the scattering mean free paths. Most modes randomize on almost the same range scale which is about $50\lambda_o$ in Figure 2.

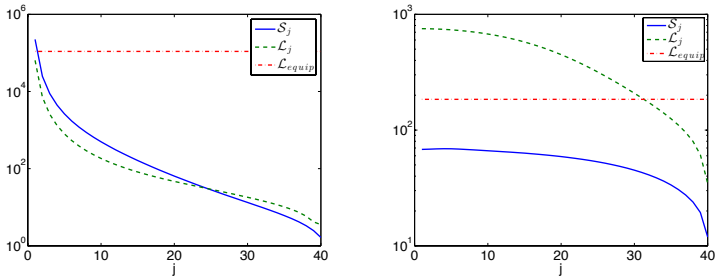

Figure 2: Left: random top boundary and right random medium. We display the scattering mean free paths (blue), dispersion scales (green) and equipartition distance (red) in units of λ_o. The abscissa is mode index.

Because of energy conservation, it is clear that at least some of the second moments of the mode amplitudes remain finite no matter how large z is. To understand this, we first determined in [3, 4] how the mode amplitudes decorrelate. We found that

$$\mathbb{E}\left[A_j(\omega,z)\overline{A_{j'}(\omega',z)}\right] \approx \mathbb{E}\left[A_j(\omega,z)\right]\overline{\mathbb{E}\left[A_{j'}(\omega',z)\right]}, \qquad \text{if } j \neq j' \text{ or } |\omega-\omega'| \gg \varepsilon^2\omega_o, \tag{11}$$

with the right hand side decaying in z as seen from (9). The waves are correlated only for small frequency offsets and for the same mode index,

$$\mathbb{E}\left[A_j(\omega,z)\overline{A_j(\omega-\varepsilon^2 h,z)}\right] \approx \sum_{q=1}^{N(\omega)} \frac{|\widehat{\rho}_q(\beta_j(\omega))|^2}{4\beta_q(\omega)\beta_j(\omega)}\widehat{W}_j^{(q)}(\omega,h,Z)e^{-i\beta_j'(\omega)\varepsilon^2 hz}, \qquad z=\varepsilon^{-2}Z, \tag{12}$$

where $W_j^{(q)}(\omega,\tau,Z)$ is the Wigner distribution and the hat denotes its Fourier transform in τ. The Wigner distribution describes the energy of the $j-$th mode at range $\varepsilon^{-2}Z$ in a time window of order $\varepsilon^{-2}\omega_o^{-1}$ centered at τ, for an initial excitation in the $q-$th mode. It satisfies a linear system of transport equations, and its Fourier transform is given by the jq entry of the matrix exponential

$$\widehat{W}_j^{(q)}(\omega,h,Z) = \left[e^{ih\mathcal{B}'Z+\Gamma Z}\right]_{jq}, \tag{13}$$

where $\mathcal{B}' = \mathrm{diag}\,(\beta_1',\ldots,\beta_N')$. The $N\times N$ real valued matrix Γ models the mixing of energy by scattering. Its off-diagonal entries are non-negative, given by

$$\Gamma_{jq} = \frac{k^4\ell}{4\beta_j\beta_q}\left[\frac{4(jq)^2}{N^4}\left(\widehat{\mathcal{R}}_{B}+\widehat{\mathcal{R}}_{T}\right)+\widehat{\mathcal{R}}_{\nu_{jq}}\right]\left(\ell\left(\beta_j-\beta_q\right)\right), \qquad j\neq q, \tag{14}$$

and its rows sum to zero $\Gamma_{jj} = -\sum_{q\neq j}\Gamma_{jq}$.

We studied extensively the properties of matrix Γ in [1], in the context of intensity based imaging of remote sources in random waveguides. That work is a direct application of the results summarized here. It quantifies explicitly the impediment of imaging caused by scattering at the boundaries and in the medium. It also introduces a robust imaging methodology. We refer to section 2 for more details.

The results described here extend to leaky waveguides, analyzed by Kohler and Papanicolaou in [18] and by Gomez in [16, 17]. From the point of view of imaging, the important difference is that there is an extra decay in the expression (13) of the Wigner distribution, due to radiation of energy through the boundaries. The results also extend to three dimensional waveguides with bounded cross-section and to electromagnetic waves. The essential difference is that there are mode degeneracies which model polarization effects, and mathematically speaking the associated amplitudes are statistically correlated (see section 1.3). Waveguides with open cross-section in one direction are different, as we explain next.

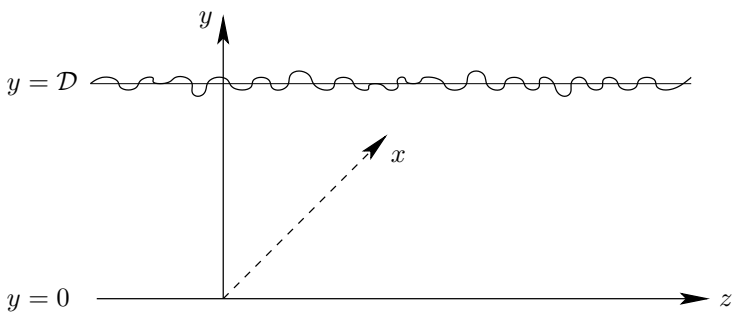

Figure 3: Schematic of the setup of our study of beam propagation in three dimensional waveguides. The system of coordinates has range origin $z = 0$ at the source. The rigid bottom boundary $y = 0$ is assumed flat and the pressure release top boundary has fluctuations around the value $y = \mathcal{D}$. The cross-range x and the range z are unbounded, i.e., $(x, z) \in \mathbb{R}^2$.

1.2 Beam propagation in random waveguides

We summarize here our results in [11], where we study wave propagation with applications to time reversal and imaging in random waveguides with unbounded cross-section. See Figure 3 for a schematic of the setup which is relevant for example to shallow underwater acoustics.

The analysis is in a long range, paraxial scaling asymptotic regime modeled with a small parameter $\varepsilon = \lambda_o/r_o \ll 1$. It is defined by the ratio of the central wavelength λ_o of the signal emitted by the source, and the beam width r_o. The beam is emitted in the range direction z and we study its propagation on the range scale L_z which is comparable to the Rayleigh length

$$L_z \sim r_o^2/\lambda_o = \varepsilon^{-2}\lambda_o \gg \lambda_o,$$

so that we can observe order one diffraction effects. To get efficient interaction of the fluctuations of the boundary with the beam, we choose their correlation length to be similar to r_o. The fluctuations have small amplitude, which is scaled so that the net scattering effects become significant at range scale L_z.

We analyze the wave field $p(t, x, y, z)$ in the random waveguide by decomposing it in waveguide modes with random amplitudes. This is similar to the decomposition (3), except that the mode amplitudes are now fields $A_j(\omega, x, z)$ that satisfy Helmholtz equations in the (x, z) plane. We show that their statistics can be described by the solution of a system of stochastic paraxial equations driven by the same Brownian motion field. We use this system to quantify explicitly the net scattering effects and calculate the following important scales:

- The mode dependent scattering mean free paths $\mathcal{S}_j$, for $j = 1, \ldots, N$. This is as explained in section 1.1 the range scale on which the mean amplitude $\mathbb{E}[A_j]$, and therefore its SNR, decays relative to its fluctuations.

- The mode dependent decoherence length $X_{d,j}$, for $j = 1, \ldots, N$. This is the cross-range scale over which the random fluctuations of the mode amplitude become statistically uncorrelated,

  $$\mathbb{E}\left[\left(A_j(\omega, x, \varepsilon^{-2}Z) - \mathbb{E}\left[A_j(\omega, x, \varepsilon^{-2}Z)\right]\right)\left(A_j(\omega, x', \varepsilon^{-2}Z) - \mathbb{E}\left[A_j(\omega, x', \varepsilon^{-2}Z)\right]\right)\right] \approx 0,$$

  for $|x' - x| > \varepsilon^{-1}X_{d,j}$. The ε scaling of the cross-range is because the beam width is $r_o = \varepsilon^{-1}\lambda_o$, with λ_o the order one length scale.

- The mode dependent decoherence frequency $\Omega_{d,j}$, for $j = 1, \ldots, N$. This is the frequency offset over which the random fluctuations of the mode amplitude become statistically uncorrelated.

We find that all three scales $\mathcal{S}_j, X_{d,j}, \Omega_{d,j}$ decrease monotonically with the mode index, meaning that the low order modes are less affected by scattering at the random boundary. This is in agreement with physics, and can be understood when associating the waveguide modes with plane waves striking the boundaries in certain directions, and reflecting there. The first modes correspond to waves that strike the boundaries at small grazing angles. They travel efficiently from the source at speed that is approximately c_o, and barely see the random boundary. This is why they are least affected by the fluctuations. The high order modes correspond to waves that strike the boundaries at almost normal incidence. They take a long path from the source and travel slowly, at much smaller speed than c_o. They interact often with the random boundary, which is why they are most affected by the fluctuations.

We quantify explicitly in [11] the dependence of S_j on the mode index. For example, we find that

$$\mathcal{S}_1 \sim \lambda_o N^4 \gg \lambda_o \quad \text{and} \quad \mathcal{S}_N \sim \lambda_o / N \ll \lambda_o,$$

where $\sim$ denotes equal up to an order one constant, and the inequalities are for high frequency regimes, with a large number N of propagating modes. Moreover,

$$X_{d,j} \sim \lambda_o \sqrt{\mathcal{S}_j / \mathcal{S}_1}, \qquad j = 1, \ldots, N.$$

Thus, the first mode amplitudes can travel at very long ranges before they lose their coherence, and their fluctuations decorrelate over cross-ranges that are similar to the beam width. The high order modes lose coherence very fast, because their scattering mean free path is short, and their fluctuations also decorrelate over cross-ranges that are much smaller than the beam width.

We use the theory of beam propagation in [11] to study time reversal and imaging in regimes of low SNR. That is, at ranges exceeding the scattering mean free paths of the modes. Our analysis of time reversal shows that super-resolution occurs, meaning that scattering at the random boundary improves the resolution of the focused field in the vicinity of the source. An essential part of the resolution analysis is the assessment of statistical stability (robustness) of the refocusing. We show that stability holds if the array has large aperture and/or the emitted signal is broadband.

Array imaging is of course more difficult than time reversal. Scattering is a serious impediment, and we need to use carefully the theory to obtain imaging methods that work in low SNR regimes. We show in [11] that imaging can be carried out by backpropagating to search points in the imaging domain local cross-correlations of the measurements of the wave field measured at the array. Local means that we cross-correlate the data projected on one mode at a time, and for nearby frequencies. We work with one mode at a time because the modes decorrelate due to scattering. Equivalently, using the plane wave analogy, we cross-correlate the waves arriving at the array from the same direction. These waves experience similar interactions with the random fluctuations, which is why their amplitudes are statistically correlated.

The imaging method in [11] is the generalization to waveguides of the Coherent Interferometric (CINT) approach that we developed with Papanicolaou and Tsogka for open environments.

1.3 Electromagnetic waveguides

Here we summarize our results in [2] on the theory of electromagnetic wave propagation in waveguides filled with a random medium with index of refraction

$$n(\vec{\mathbf{x}}) = \frac{c_o}{c(\vec{\mathbf{x}})} = \left[1 + \varepsilon \nu(\vec{\mathbf{x}})\right]^{1/2},$$

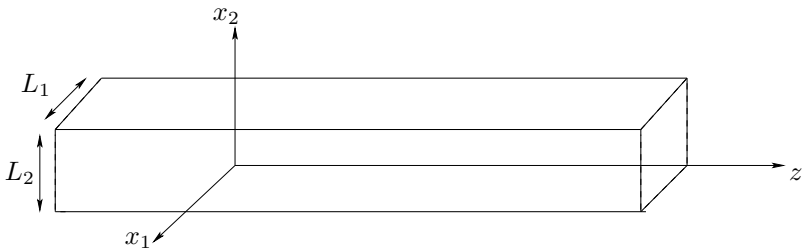

Figure 4: Schematic of the rectangular waveguide used to analyze electromagnetic wave propagation.

defined by the ratio of the reference electromagnetic wave speed c_o and the perturbed speed $c(\vec{\mathbf{x}})$. The fluctuations are modeled by the mean zero random process ν, which is stationary in z, with z integrable autocorrelation $\mathcal{R}_\nu$. The waveguide has perfectly conducting walls and rectangular cross-section $(0, L_1) \times (0, L_2)$, as illustrated in Figure 4. This is to obtain an explicit quantification of the net scattering effects on the wave field, the solution of Maxwell's equations

$$\vec{\nabla} \times \vec{\mathbf{H}}(\omega, \vec{\mathbf{x}}) = \vec{\boldsymbol{\mathcal{J}}}(\omega, \mathbf{x})\delta(z) - i\omega\vec{\mathbf{D}}(\omega, \vec{\mathbf{x}}) \tag{15}$$

$$\vec{\nabla} \times \vec{\mathbf{E}}(\omega, \vec{\mathbf{x}}) = i\omega\mu_o\vec{\mathbf{H}}(\omega, \vec{\mathbf{x}}) \tag{16}$$

$$\vec{\nabla} \cdot \vec{\mathbf{H}}(\omega, \vec{\mathbf{x}}) = 0 \tag{17}$$

$$\vec{\nabla} \cdot \vec{\mathbf{D}}(\omega, \vec{\mathbf{x}}) = \varrho(\omega, \vec{\mathbf{x}}), \tag{18}$$

for $\vec{\mathbf{x}} = (\mathbf{x}, z)$, with $\mathbf{x} \in (0, L_1) \times (0, L_2)$ and $z \in \mathbb{R}$. Here $\vec{\mathbf{E}}$ and $\vec{\mathbf{D}}$ are the electric field and displacement, $\vec{\mathbf{H}}$ is the magnetic field and μ_o is the magnetic permeability, assumed constant. The source excitation is modeled by the current density $\vec{\boldsymbol{\mathcal{J}}}(\omega, \mathbf{x})\delta(z)$ localized at the origin of range, and $\varrho(\omega, \vec{\mathbf{x}})$ is the charge density.

Similar to the acoustic case (section 1.1), we analyze the wave field by decomposing it into modes, solutions of Maxwell's equation of the form

$$(\mathbf{E}, E_z)(\omega, \mathbf{x}, \pm\beta)e^{\pm i\beta z} \quad \text{and} \quad (\mathbf{H}, H_z)(\omega, \mathbf{x}, \pm\beta)e^{\pm i\beta z}.$$

The decomposition involves calculating the spectrum of a vector Laplacian, which has a countable set of eigenvalues with square root defining the wavenumbers β. The eigenvalues are not simple, and the associated mode degeneracy models the polarization effects.

To satisfy exactly the boundary conditions, at all orders of the asymptotic parameter ε, we work explicitly with the cross-range components of the electric displacement

$$\mathbf{D}(\omega, \vec{\mathbf{x}}) = \sum_{j=1}^{N(\omega)} \sum_{s=1}^{\mathfrak{M}_j} \boldsymbol{\varphi}_j^{(s)}(\mathbf{x}) \left(\sqrt{\frac{k}{\beta_j(\omega)}}\delta_{s1} + \sqrt{\frac{\beta_j(\omega)}{k}}\delta_{s2} \right) \left(A_j^{(s)}(\omega, z)e^{i\beta_j(\omega)z} + B_j^{(s)}(\omega, z)e^{-i\beta_j(\omega)z} \right) + \text{evanescent.} \tag{19}$$

Then $\mathbf{H} = c_o\mathbf{U}^\perp$, where $\mathbf{U}$ is the rotated and scaled magnetic field, with decomposition

$$\mathbf{U}(\omega, \vec{\mathbf{x}}) = \sum_{j=1}^{N(\omega)} \sum_{s=1}^{\mathfrak{M}_j} \boldsymbol{\varphi}_j^{(s)}(\mathbf{x}) \left(\sqrt{\frac{\beta_j(\omega)}{k}}\delta_{s1} + \sqrt{\frac{k}{\beta_j(\omega)}}\delta_{s2} \right) \left(A_j^{(s)}(\omega, z)e^{i\beta_j(\omega)z} - B_j^{(s)}(\omega, z)e^{-i\beta_j(\omega)z} \right) + \text{evanescent.} \tag{20}$$

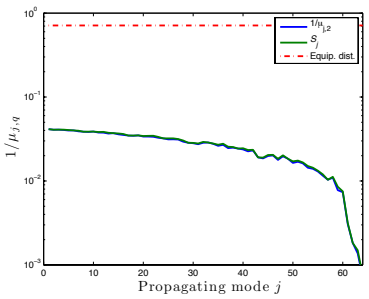

Figure 5: Scattering mean free paths (green curve) for electromagnetic waves in a random waveguide with rectangular cross-section.

The longitudinal components D_z and H_z are determined by $\mathbf{D}$ and $\mathbf{H}$, as follows from Maxwell's equations. The decomposition (19) is similar to that in acoustics (equation (3)), except that for each wavenumber β_j, there are multiple eigenfunctions $\boldsymbol{\varphi}_j^{(s)}(\mathbf{x})$ of the vector Laplacian. The multiplicity is denoted by $\mathfrak{M}_j$ and by choosing L_2/L_1 irrational we can restrict it to $1 \leq \mathfrak{M}_j \leq 2$. This is in order to be able to carry a quantitative analysis of the statistics of the mode amplitudes $A_j^{(s)}$ and $B_j^{(s)}$.

Our results in [2] are:

- Rigorous analysis of the coupling between the forward, backward and evanescent waves. Proof that when the autocorrelation $\mathcal{R}_\nu$ of the medium fluctuations is smooth in z, the forward scattering approximation holds.
- Complete characterization of the statistics of the mode amplitudes A_j at long ranges $z = \varepsilon^{-2}Z$, with $Z \gtrsim \lambda_o$, where there are net scattering effects.
- Calculation of the scattering mean free paths of the modes, the range scales on which they randomize. See Figure 5 and compare with the right plot in Figure 2 to note the similarity of the behavior of the scattering mean free paths in acoustics.
- Proof that modes with different wavenumber are statistically decorrelated, as in the acoustic case. The frequency decorrelation is of order $\varepsilon^2\omega_o$, as well.
- Analysis of the transport of energy by the modes. This is the most challenging part of the project because it involves studying the z evolution of the $\mathfrak{M}_j \times \mathfrak{M}_j$ Hermitian matrices with entries $\mathbb{E}\left[A_j^{(s)}\overline{A_j^{(s')}}\right]$ for $1 \leq s, s' \leq \mathfrak{M}_j$. In the acoustic case the energies where scalar. Here they are matrices due to the mode degeneracy (polarization effects). We established rigorously in [2] under which conditions waves reach the equipartition regime. It remains to understand how the off-diagonal entries of the Hermitian energy matrices decay, which is the mathematical manifestation of the wave depolarization. Understanding this is crucial for imaging applications.

2 Imaging in random waveguides

Here we describe the results in [12, 1] for imaging in two dimensional acoustic waveguides. The results extend to electromagnetic waveguides, once we understand how the waves depolarize (see last item above).

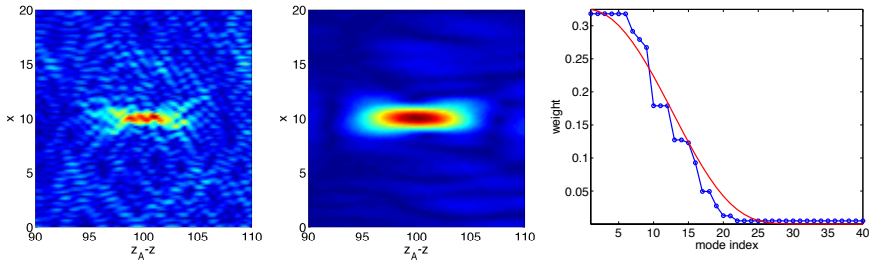

Figure 6: Adaptive coherent imaging results for a point source at range $100\lambda_o$ from an array of receivers, in waveguide with top random, pressure release boundary. Image with no mode filtering (left) and with adaptive mode filtering (middle). The theoretical mode weights (red) agree with the numerical ones (blue) in the right plot.

The study in [12] is concerned with the formulation and analysis of a novel coherent imaging approach with adaptive mode filtering. It applies to waveguides with random boundaries where there is strong mode dependence of the scattering mean free paths, as illustrated in the left plot of Figure 2. The algorithm determines during the image formation which modes are incoherent (i.e., for which j we have $z > \varepsilon^{-2}\mathcal{S}_j$), and filters them out. It images by time reversing the received wave, weighting the modes based on their being coherent or not, and backpropagating them to the search domain in the ideal waveguide. We illustrate in Figure 6 the results for the same waveguide considered in the left plot of Figure 2. The image on the left is obtained with the standard approach, which uses all the recorded modes. It is not bad, as half of the modes are coherent, but it is a bit noisy. The image in the middle is with optimal mode weighting. The weights are shown in the right plot. Note how the numerically computed weights (blue line) match those computed analytically (red). Note also that the algorithm estimates that only the first twenty modes are coherent, which agrees with what the left plot in Figure 2 says: the source range $100\lambda_o \lesssim \mathcal{S}_j$ for $1 \leq j \leq 20$. This demonstrates that our theory is quantitative.

The study in [1] applies to a much stronger scattering regime, where all the modes are incoherent, meaning that the array is at range $z > \varepsilon^{-2}\mathcal{S}_1$. It estimates the mode energies from the array measurements and uses the transport theory summarized in section 1.1 to invert for the source density ρ and its range z. The mode energies are defined by

$$\mathcal{C}_j(\tau) = \frac{2\pi H}{\varepsilon^2} \int dt\, \psi(Ht) \left| D_j\left(\frac{\tau - t}{\varepsilon^2}\right)\right|^2 \approx \mathbb{E}[\mathcal{C}_j(\tau)], \tag{21}$$

and we show that they are self-averaging when the bandwidth is large with respect to the decoherence frequency of order $\varepsilon^2\omega_o$. We assume in [1] that

$$\varepsilon^2\omega_o \ll B \ll \omega_o, \tag{22}$$

so that we can freeze the number of modes in the bandwidth to $N(\omega_o)$. However, as we explain at the end of this section, a larger bandwidth may be beneficial, in which case we can divide it in sub-bands satisfying the relation (22). In definition (21) $D_j(t)$ is the data projected on the $j-$th mode

$$D_j(t) = \int_0^X dx\, 1_{\mathcal{A}}(x)\, \phi_j(x)\, p(t, x, z), \tag{23}$$

where $1_{\mathcal{A}}(x)$ is the indicator function of the array aperture $\mathcal{A}$, and ψ is a bump function (smooth, compactly supported in an interval of order one). We anticipate the time to be of order $\varepsilon^{-2}\tau$ in (21) because the range

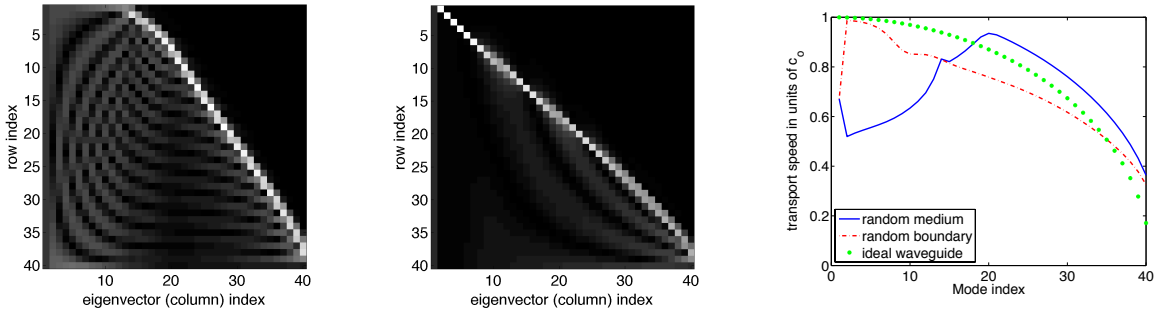

Figure 7: Left: matrix of eigenvectors of Γ for a waveguide filled with a random medium. Middle: matrix of eigenvectors of Γ for a waveguide with random top boundary. The autocorrelation of the fluctuations is Gaussian in both cases and $\ell = 3\lambda_o$. We display the absolute values of the entries. White indicates high values and black nearly zero values. Right: the transport speed v_r in the waveguide with random medium (blue), with random boundary (red) and in ideal waveguide (green).

is $z = \varepsilon^{-2}Z$, and scale t similarly in the argument of the data. This implies that we cross-correlate the measurements at frequency offsets $\varepsilon^2 h$, with $|h| \le H < \omega_o$, where the theory tells us that the waves are statistically correlated.

The mathematical model of $\mathcal{C}_j(\tau)$ turns out to be

$$\mathcal{C}_j(\tau) \approx \frac{\|f\|^2}{4B} \sum_{q,l=1}^{N} Q_{jq}^2 \frac{|\widehat{\rho}_l\,[\beta_q]|^2}{\beta_l \beta_q} \int \frac{dh}{2\pi} \widehat{\psi}\left(\frac{h}{H}\right) \left[e^{(ih\mathcal{B}'+\Gamma)Z}\right]_{ql} e^{-ih\tau}, \tag{24}$$

with $N \times N$ matrices $\mathcal{B}'$ and Γ defined in section 1.1, and coupling matrix due to the array aperture

$$Q_{jq} = \int_0^X dx\, 1_{\mathcal{A}}(x)\phi_j(x)\phi_q(x), \qquad j,q = 1,\ldots,N. \tag{25}$$

The unknowns in (24) are the scaled range Z of the source and the source density, which appears as the absolute value of its Fourier coefficients.

The range Z can be determined from the arrival times of $\mathcal{C}_j(\tau)$. It turns out that these can be estimated using perturbation theory, because in forward scattering approximation regimes $ih\mathcal{B}'$ may be treated as a perturbation of Γ. Let Λ_j and $\mathbf{u}_j$ denote the eigenvalues and orthonormal eigenvectors of the symmetric matrix Γ, and assume that the eigenvalues are simple. They are necessarily non-positive, or else the energy cannot be conserved, and we order them as $0 = \Lambda_1 > \ldots \Lambda_N$. Regular perturbation theory allows us to rewrite (24) as

$$\mathcal{C}_j(\tau) \approx \frac{H\|f\|^2}{4B} \sum_{r=1}^{N} e^{-|\Lambda_r|Z}\, \Psi\left(H(\tau - Z/v_r)\right) \sum_{q,l=1}^{N} Q_{jq}^2 \frac{|\widehat{\rho}_l\,[\beta_q]|^2}{\beta_l \beta_q} \left(\mathbf{u}_r \mathbf{u}_r^T\right)_{ql}, \tag{26}$$

with

$$v_r = (\mathbf{u}_r^T \mathcal{B}' \mathbf{u}_r)^{-1} = \left(\sum_{j=1}^{N} \beta_j' u_{jr}^2\right)^{-1} \neq 1/\beta_r'. \tag{27}$$

Thus, we see a superposition of the bumps ψ traveling at transport speeds v_r, which are different than the speeds $1/\beta_r'$ in ideal waveguides, unless $\mathbf{u}_r$ are close to the basis vectors $\mathbf{e}_r$. See Figure 7 for an illustration

of the anomalous dispersion of the transport speed. Note in particular that the dominant entry in (26), for $r = 1$, which doesn't decay in range, is transported at the average speed

$$v_1 = \left(\frac{1}{N} \sum_{j=1}^{N} \beta_j' \right)^{-1}, \tag{28}$$

because $\mathbf{u}_1 = (1, \ldots, 1)^T/\sqrt{N}$. We explain in [1] how to use the anomalous dispersion and the transport model to estimate the range $z = \varepsilon^{-2} Z$ of the source and also the matrix Γ. The latter requires some knowledge of the model of the autocorrelation.

After estimating the range (and Γ), we can recover information about the source density ρ from the vector $\mathbf{M} = (M_1, \ldots, M_N)^T$ of the time integral of the intensities (24), where

$$M_j := \frac{4B}{\|f\|^2 \widehat{\psi}(0)} \int_{-\infty}^{\infty} d\tau \, \mathcal{C}_j(\tau), \qquad j = 1, \ldots, N. \tag{29}$$

Suppose the density is separable $\rho(x, z) = \xi(x)\zeta(z)$ and, let $\mathbb{Q} = \left(Q_{jq}^2\right)$ to write

$$\mathbf{M} \approx \mathbb{Q} \, \mathrm{diag} \left(\frac{|\widehat{\zeta}(\beta_1)|^2}{\beta_1}, \ldots, \frac{|\widehat{\zeta}(\beta_N)|^2}{\beta_N} \right) \sum_{j=1}^{N} e^{-|\Lambda_j| Z} \left[\mathbf{u}_j^T \begin{pmatrix} |\widehat{\xi}_1|^2/\beta_1 \\ \vdots \\ |\widehat{\xi}_N|^2/\beta_N \end{pmatrix} \right] \mathbf{u}_j, \tag{30}$$

where N and the wavenumbers are evaluated at the central frequency ω_o. There is not enough data to find both ξ and ζ. Typically in imaging the range is estimated from travel time. In our case the travel time resolution is $O(\varepsilon^{-2} H^{-1})$, so we cannot estimate the range beyond the scale $\varepsilon^{-2} Z$. We map all the range density at the center of the source $\zeta(z) \rightsquigarrow \delta(z)$ and seek to estimate the cross-range density $\xi(x)$. At best we can only get $(|\widehat{\xi}_j|)_{1 \le j \le N}$ from which we can estimate the support of $\xi(x)$, as explained in [1].

To find $(|\widehat{\xi}_j|)_{1 \le j \le N}$ from (30) means inverting the matrix exponential. This is unstable (expected ill-posedness of any transport based inversion), so we regularize to obtain

$$\left(|\widehat{\xi}_1|^2/\beta_1, \ldots |\widehat{\xi}_N|^2/\beta_N \right)^T \overset{?}{\approx} \sum_{j=1}^{J} e^{|\Lambda_j| Z} \left(\mathbf{u}_j^T \mathcal{B} \mathbb{Q}^{-1} \mathbf{M} \right) \mathbf{u}_j, \tag{31}$$

for J chosen so that $Z \gg 1/|\Lambda_j|$ for $j > J$. We analyze this result in [1] and show that (31) approximates the first J components of the left hand-side if J is not too low (i.e., the range is not too large). This is because the matrix of eigenvectors has a nearly vanishing upper right corner (see the plots in Figure 7 and the analysis in [1]). However, for larger and larger range (31) does not approximate the left hand side. In particular, when $Z \gg 1/|\Lambda_2|$, we note from (30) that

$$\mathbf{M} \approx \left(\frac{1}{N} \sum_{j=1}^{N} \frac{|\xi_j|^2}{\beta_j} \right) \mathbb{Q}(1, \ldots, 1)^T, \tag{32}$$

so all we can get from the inversion is the average of the absolute values of the Fourier coefficients. The scale

$$\mathcal{L}_{eq} = \frac{1}{|\Lambda_2|} \tag{33}$$

is called the equipartition distance, because it is the range at which the energy is uniformly distributed over the modes by scattering, no matter the initial condition. Cross-range estimation from narrowband data is

impossible in the equipartition regime. See figure 2 for a comparison between the equipartition distance (red line) and the scattering mean free paths (blue curve). Note how $\mathcal{L}_{eq}$ exceeds $\mathcal{S}_1$ by an order of magnitude in the waveguide filled with random media (right plot), indicating that transport based inversion is useful. When the random boundary effects dominate (left plot) we have $\mathcal{L}_{eq} \approx \mathcal{S}_1$, meaning that once all the modes become incoherent, they are also in equipartition. Transport based inversion is not useful in these waveguides, at least not for narrowband data.

Broadband data can improve the source estimation even when the waves are in equipartition, as we show in [1]. This is because when the frequency changes, both the number $N(\omega)$ and the wavenumbers β_j (weights in (32)) change, thus allowing us to get some information about the cross-range profile of the source.

In any case, the transport based inversion cannot be expected to give very detailed information about the source density, because it can only give the absolute value of the Fourier coefficients of its cross-range profile. In the electromagnetic case we expect an improvement, due to polarization (i.e., mode degeneracy). There we deal with Hermitian energy matrices whose off-diagonal entries bring phase information about the Fourier coefficients of the unknown source density.

3 Pulse propagation in time dependent random media

Here we describe the results in [14], which are concerned with the evolution of a pulse while traveling in a time dependent random medium. As far as we know, this is the first study that takes rigorously into account rapid time changes.

The analysis is for acoustic waves in layered media, modeled by the first order system

$$\begin{aligned} \varrho \partial_t u(t,z) + \partial_z p(t,z) &= f(t)\delta(z), \\ \frac{1}{K(t,z)} \partial_t p(t,z) + \partial_z u(t,z) &= 0, \end{aligned} \tag{34}$$

where ϱ is the mass density assumed constant, K is the bulk modulus, p is the pressure, u is the vertical displacement velocity, and f is the pulse emitted by the source at $z = 0$. The wave speed $c(t,z) = \sqrt{K(t,z)/\varrho}$ in the random medium is modeled by

$$\frac{1}{c(t,z)} = \begin{cases} \left[1 + \sigma\nu\left(\frac{t}{T}, \frac{z}{\ell}\right)\right]/c_o, & z > 0, \\ 1/c_o & \text{otherwise}, \end{cases} \tag{35}$$

where ν is a mean zero stationary random process in both arguments, ℓ is the correlation length, T is the correlation time and σ quantifies the amplitude of the fluctuations. The analysis is in the following scaling regime defined using the reference range scale of propagation L. We take

$$\varepsilon^2 = T_f/(L/c_o) \ll 1, \qquad \sigma = \varepsilon, \tag{36}$$

where T_f is the duration of the pulse, so the wavelength λ_o is of order $\varepsilon^2 L$. The correlation length ℓ and time T are defined by

$$T = \varepsilon^{\alpha-2} T_f, \qquad \ell = \varepsilon^\beta L, \tag{37}$$

where we vary α and β to distinguish between two interesting regimes where the random medium plays a role: Slowly changing media, where $\alpha < 2$ and $\beta = 2$ and rapidly changing media, where $\alpha = 2$ and $\beta \leq 2$.

The main results are:

- Derived a Volterra integral equation for the wave front which describes the evolution of the pulse shape.

- Obtained a new averaging result for this equation in coordinates centered at a random time, to prove that the pulse shape is deterministic.
- Described in detail the pulse deformation and showed that rapid time variations in the medium may feed energy into the pulse, and thus prevent fading. For slow time changes the pulse behaves as in time independent media. It broadens and fades as described by the well known O'Doherty-Anstey theory.

4 SAR imaging

Here we summarize the work in [8, 7], which aims to introduce and analyze from first principles a synthetic aperture radar (SAR) imaging methodology that can be combined with target motion estimation and autofocus. This involves two main steps:

1. The first step is a segmentation of the data into small, properly calibrated sub-apertures. Such apertures are essential in motion estimation, where we wish to approximate the target motion as a uniform translation over small time intervals defining the sub-aperture. Small apertures are also important in image formation and other data processing, because they allow linearization of phases in the slow time, which means that calculations can be done with the fast Fourier transform.
2. The second step is data processing for extracting target motion and platform trajectory perturbations.

We have shown in our previous work [6] with analysis and numerical simulations how this can be done in the phase space, using Wigner transforms and ambiguity functions. The phase space approach works for a single target or for groups of targets that are in similar motion (either all of them are stationary or they move at the same speed). Moreover, it can only determine the relative motion of the targets with respect to the platform. That is to say, the phase space approach by itself cannot handle complex scenes and it does not decouple motion estimation from autofocus.

To decouple motion estimation from autofocus, we need complex scenes. To deal with them, we have introduced a data filtering approach that seeks to divide the SAR data into subsets corresponding to targets that are stationary and/or in similar motion. Then, the phase space approach can be used separately on these subsets to carry out the autofocus and to estimate target motion. The data filters are based on travel time transformations (delays) applied to the pulse compressed SAR data. The filters are extensions of ideas in our paper [9]. We have also shown that travel time transformations can also be used to estimate target velocities in a two step, one dimensional optimization procedure, that determines separately the velocity in the range direction and in the cross-range direction.

The separation of the pulse compressed SAR echoes from stationary targets and moving targets can also be done with the robust principal analysis (PCA) approach. This requires however appropriate windowing of the data. A careful theoretical and numerical study of filtering with robust PCA is in [8].

5 Work in progress

We are currently working with Ilker Kocyigit (AFOSR supported postdoc) on understanding sparsity based optimization imaging methods in random media, and with Liem Dinh Nguyen (AFOSR supported postdoc) on imaging with electromagnetic waves in terminating waveguides. Moreover, we study with Derek Wood (graduate student, not supported by AFOSR) wave propagation in turning waveguides.

II. Other activities and findings

- In [13] we studied the Dirichlet to Neumann map of composite media with highly conducting inclusions packed at high volume. We presented a constructive method of approximation which can be used in numerics to obtain efficient preconditioners for domain decomposition methods.
- In [10] we introduced a novel inversion approach for parabolic equations, based on model reduction. The equation arises in controlled source electromagnetic inversion. We analyzed theoretically the algorithm and assesed its performance using numerical simulations.
- The solicited article [5] is a review of imaging in random media which will appear in the Handbook of Mathematical Methods in Imaging published by Springer.
- The research in Alonso, R., and Lods, B.: Boltzmann model for viscoelastic particles Asymptotic behavior, pointwise lower bounds and regularity., accepted for publication in Comm. Math. Phys. (2014), was done while Ricardo Alonso was an AFOSR supported postdoc.
- The following research of Sebastian Acosta was done while he was an (AFOSR supported student) :
  A control approach to recover the wave speed (conformal factor) from one measurement. Submitted 2014. Preprint arXiv:1401.6737
  Recovery of the absorption coefficient in radiative transport from a single measurement. Submitted 2014. Preprint arXiv:1308.4655v2.
  Time reversal for radiative transport with applications to inverse and control problems. Inverse Problems 29: 085014, 2013.

III. Broader impact

Students advised:

1. Wang Yingpei, Rice University PhD 2014. Thesis topic: *Imaging in high contrast media.* Now at Oracle, San Francisco.
2. Sebastian Acosta, Rice University PhD 2014. Project: *Inverse source problems for time-dependent radiative transport in scattering media.* Now postdoc at Baylor College of Medicine, Houston.
3. Derek Wood, University of Michigan, 3rd year PhD student. Working on wave propagation in turning random waveguides.

Postdocs advised:

1. Ricardo Alonso, PhD 2008, Mathematics, UT Austin. Supported by AFOSR. Currently assistant professor at Pontificia Universidade Católica Rio de Janeiro, Brazil.
2. Thomas Callaghan, PhD 2010, Institute of Computational Mathematics and Engineering (ICME), Stanford University. NSF VIGRE postdoc. Project: SAR imaging with motion estimation and autofocus. Currently quantitative researcher at Quantres, Bahamas.
3. 2013-2017 Ilker Kocyigit at University of Michigan, PhD 2013 in Mathematics from University of Washington, Seattle. Supported by AFOSR and working on optimization based imaging in random media.
4. 2013-2017 Liem Nguyen at University of Michigan, PhD 2013 in Mathematics from Ecole Polytechnique. Supported by AFOSR and working on imaging in terminating waveguides.

Publications references [1-8] and [10-14].

Invited presentations

1. *Imaging with waves in complex environments*, PIMS/UBC/IAMS Distinguished Colloquium, Vancouver, BC, October 31, 2014.
2. *Imaging in random media* (plenary lecture), Conference in Inverse Problems and Spectral Theory, Oct 17-19, 2014, Texas A&M University, College Station, TX.
3. *Imaging with waves in complex environments* (plenary lecture), Continuum Models Discrete Systems - 13 Conference, Salt Lake City, Utah, July 21-25, 2014.
4. *Imaging with waves in complex environments* (plenary lecture), workshop on Theoretical and Applied Computational Inverse Problems, Schrödinger Institute, Vienna, Austria, May 5-16, 2014.
5. *Imaging with waves in complex environments*, Applied Mathematics Colloquium, Harvard University, Cambridge, April 7, 2014.
6. *Electromagnetic wave propagation in random waveguides*, Applied Mathematics Colloquium, Stanford University, March 5, 2014.
7. *A quantitative study of imaging in random waveguides*, CSP Seminar, Electrical Engineering Department, University of Michigan, February 20, 2014.
8. *The Dirichlet to Neumann map of high contrast media*, Applied Interdisciplinary Mathematics seminar, Nov. 1, 2013, Department of Mathematics, University of Michigan, Ann Arbor.
9. *The Dirichlet to Neumann map of high contrast media*, colloquium Oct 24, 2013, Department of Mathematics, University of Illinois, Urbana Champaign.
10. *A quantitative study of imaging in random waveguides* (plenary lecture) International conference on novel directions in inverse scattering, July 29 - August 2, 2013, University of Delaware.
11. *An asymptotic study of the Dirichlet to Neumann map of high contrast conductive media*, colloquium Jun 14, 2013, Ecole Normale Superieure, Paris.
12. *An asymptotic study of the Dirichlet to Neumann map of high contrast conductive media* (plenary lecture), Conference on Applied Analysis for the matherial sciences, May 27-31, 2013, CIRM Lumini, Marseille.
13. *Paraxial coupling of waves in 3-D random waveguides* (plenary lecture), Recent developments in applied Mathematics, Conference in honor of George Papanicolaou's 70th birthday, January 24-27, 2013, Stanford, CA.
14. *Paraxial coupling of waves in 3-D random waveguides* (plenary lecture), Workshop on Theory and Applications of Stochastic PDE's, January 14-18, 2013, IMA, Minneapolis.

Editorial positions 2012-2013:

1. Editorial board SIAM Journal on Multiscale Modeling and Simulations.
2. Editorial board SIAM Journal on Uncertainty Quantification.
3. International Advisory Panel of the Journal Inverse Problems

National committees:

1. Elected member of the SIAM Council, 2014-2017.
2. Member of SIAM Coordinating Committee of Joint Mathematics Meeting (2014-2017).
3. Member of the SIAM Imaging Science best paper award committee, 2013.
4. Elected member at large of the Inverse Problems International Association.

Advisory boards:

1. International Scientific Advisory Board of the National Academy of Finland, for the Center of Excellence in Inverse Problems Research, 2012-2017.
2. Member of the Scientific Review Panel for the Pacific Institute for the Mathematical Sciences, UBC, Vancouver, Canada.

Honors and awards:

1. 2015 Simons Fellow in Mathematics.
2. Peter Field Collegiate Chair Professor in the Department of Mathematics, University of Michigan, Ann Arbor. Starting date: September 1, 2013.

References

[1] S Acosta, R Alonso, and L Borcea. Source estimation with incoherent waves in random waveguides. to appear in Inverse Problems. Preprint arXiv:1408.1937v1., 2015.

[2] R Alonso and L Borcea. Electromagnetic wave propagation in random waveguides. Under review at SIAM Multiscale Model. Simul. Preprint arXiv:1310.4890v1, 2014.

[3] R Alonso, L Borcea, and J Garnier. Wave propagation in waveguides with random boundaries. *Communications in Mathematical Sciences*, 11(1):233–267, 2012.

[4] L. Borcea. Imaging and wave propagation in random waveguides. Lecture notes Panorama et Synthése published by Societé Mathematique de France, in press, 2014.

[5] L. Borcea. Imaging in random media. In Otmar Scherzer, editor, *Handbook of Mathematical Methods in Imaging*, page 2000. Springer, 2016.

[6] L Borcea, T Callaghan, and G Papanicolaou. Synthetic aperture radar imaging with motion estimation and autofocus. *Inverse Problems*, 28(4):045006, 31 pp., 2012.

[7] L Borcea, T Callaghan, and G Papanicolaou. Motion estimation and imaging of complex scenes with synthetic aperture radar. *Inverse Problems*, 29(5):054011, 29 pp., 2013.

[8] L Borcea, T Callaghan, and G Papanicolaou. Synthetic aperture radar imaging and motion estimation via robust principal component analysis. *SIAM J. Imaging Science*, 6(3):1445–1476, 2013.

[9] L. Borcea, F. González del Cueto, G. Papanicolaou, and C. Tsogka. Filtering deterministic layering effects for imaging. *SIAM Review*, 54:757–798, 2012.

[10] L Borcea, V Druskin, A Mamonov, and M Zaslavsky. A model reduction approach to numerical inversion for a parabolic partial differential equation. *Inverse Problems*, 30(12):125011, 2014.

[11] L Borcea and J Garnier. Paraxial coupling of propagating modes in three-dimensional waveguides with random boundaries. *SIAM Multiscale Model. Simul.*, 12(2):832–878, 2014.

[12] L Borcea, J Garnier, and C Tsogka. A quantitative study of source imaging in random waveguides. *Comm. Math. Sci.*, 2014. in press. Preprint arXiv: 1306.1544v1.

[13] L Borcea, Y Gorb, and Y Wang. Asymptotic approximation of the Dirichlet to Neumann map of high contrast conductive media. *SIAM Multiscale Model. Simul.*, 2014. in press. Preprint arXiv: 0760149.

[14] L Borcea and K Solna. Pulse propagation in randomly layered media. submitted to SIAM Multiscale Model. Simul. Preprint arXiv:1408.3749v1., 2014.

[15] L. B. Dozier and F. D. Tappert. Statistics of normal mode amplitudes in a random ocean. *Journal of the Acoustical Society of America*, 63:533–547, 1978.

[16] C. Gomez. Wave propagation in shallow-water acoustic random waveguides. *Commun. Math. Sci.*, 9:81–125, 2011.

[17] C. Gomez. Loss of resolution for the time reversal of wave in underwater acoustic random channels. *Math. Mod. Meth. App. Sci.*, 23(11):2065–2110, 2013.

[18] W. Kohler and G. Papanicolaou. *Wave Propagation and Underwater Acoustics, J. B. Keller and J. S. Papadakis, eds.*, volume 70 of *Lecture Notes in Physics*, chapter Wave propagation in randomly inhomogeneous ocean. Springer Verlag, Berlin, 1977.